A Mesodermal Fate Map for Adipose Tissue

Zachary L. Sebo[1], Elise Jeffery[5], Brandon Holtrup[1] and Matthew S. Rodeheffer[1-4]

Yale University, Department of Molecular, Cellular and Developmental Biology[1], Department of Comparative Medicine[2], Yale Stem Cell Center[3], Yale Program in Integrative Cell Signaling and Neurobiology of Metabolism[4], and Yale Department of Cell Biology[5]

Summary: Embryonic cell lineage tracing of adipose tissue reveals that perigonadal fat arises from distinct mesodermal subcompartments in males and females and that less than 50% of interscapular brown fat arises from central dermomyotome.

Key words: adipocyte, adipose, development, fate map, lineage tracing, mesoderm

Correspondence should be addressed to:
Matthew Rodeheffer
matthew.rodeheffer@yale.edu
of Comparative Medicine
Yale University School of Medicine
375 Congress Ave
New Haven, CT 06520
Tel #203-737-3370
Fax #203-785-7499

Abstract

The embryonic origin of distinct fat depots and the role for ontogeny in specifying the functional differences among adipocyte lineages between and within depots is unclear. Using a Cre/Lox-based strategy to track the fate of major mesodermal subcompartments in mice we present evidence that fewer than 50% of interscapular brown adipocytes are derived from progenitors of the central dermomyotome. Furthermore, we demonstrate that depot-specific adipocyte lineages spatially diverge as early as gastrulation and that perigonadal adipocytes arise from separate mesodermal subcompartments in males and females. Last, we show adipocyte precursors (APs) of distinct lineages within the same depot exhibit indistinguishable responses to a high fat diet, indicating ontogenetic differences between APs do not necessarily correspond to functional differences in this context. Altogether, these findings shed light on adipose tissue patterning and suggest the behavior of adipocyte lineage cells is not strictly determined by developmental history.

Introduction

Appropriate developmental patterning of adipose tissue results in a stereotyped anatomical configuration of white and brown fat depots. The main white adipose tissue (WAT) depots are positioned within the abdominal cavity (i.e. viscerally) and subcutaneously around the hips and thighs, whereas brown adipose tissue (BAT) is predominately constrained to interscapular and thoracic regions of the body (Cypess et al., 2009; de Jong et al., 2015; Lee et al., 2013; Nedergaard et al., 2007; Shen et al., 2003). The primary role of WAT is to store energy in the form of triglycerides while BAT metabolizes fatty acids, producing heat (Cannon and Nedergaard, 2004; Rosen and Spiegelman, 2014). Proper WAT and BAT function depends on constituent endothelial, hematopoietic and fibrotic cell populations (Khan et al., 2009; Marcelin et al., 2017; Rupnick et al., 2002; Xu et al., 2003). However, the defining feature and essential unit of all adipose tissue is the adipocyte. These 'fat cells' are known to arise from depot-resident adipocyte precursors (APs) in adults (Berry and Rodeheffer, 2013; Rodeheffer et al., 2008), yet the embryonic progenitor pools from which depot-specific adipocyte lineages originate are not clear.

Early studies suggested that brown adipocytes arise from progenitors residing in the central dermomyotome, a subcompartment of somites that makes important contributions to the dorsal dermis and epaxial muscle (Atit et al., 2006; Lepper and Fan, 2010; Seale et al., 2008). From these data it was inferred that BAT and WAT are derived from completely distinct embryonic progenitor pools. However, the tracing systems leveraged to make these conclusions utilized cytoplasmic markers which have since been shown to be ineffective for labeling adipocytes (Jeffery et al., 2014; Sanchez-Gurmaches et al., 2016). More recent data utilizing membrane-targeted fluorescent markers coupled to the Myf5- and Pax3-Cre drivers (Lang et al., 2005; Tallquist et al., 2000) indicate that several major BAT depots and, surprisingly, WAT depots share a common origin in the somites (Sanchez-Gurmaches and Guertin, 2014). Despite this progress, the particular regions within the somites from which these depots arise and the lineage hierarchy of the progenitors involved remain undetermined.

A similar strategy with the inducible WT1-CreER^{T2} driver (Zhou et al., 2008) was used to show that the visceral but not subcutaneous adipocyte lineage arises from embryonic mesothelial cells, which line organs of the abdominal cavity late in gestation (Chau et al., 2014). In a complementary study the subcutaneous adipocyte lineage was selectively labeled when limb bud mesenchyme was traced by Prx1-Cre (Logan et al., 2002; Sanchez-Gurmaches et al., 2015). Taken together, these observations indicate that visceral and subcutaneous adipocyte lineages are segregated by late embryogenesis. However, to identify the time period and embryonic subdomain in which this lineage bifurcation takes place tracing from earlier time points is required.

Here we use a somite-specific driver, Meox1-Cre (Jukkola et al., 2005), to show that white and brown adipocyte lineages that populate dorso-axial depots, along with a major proportion of the male perigonadal lineage, are derived from somitic mesoderm. We show that a subpopulation of interscapular white and brown adipocytes arise from Pax7^{+} progenitors and integrate this observation with data from previous reports to argue that the epaxial dermomyotome, not the central dermomyotome, is the major source for interscapular adipocytes. We use constitutive and inducible Cre/Lox systems to track the fate of posterior lateral plate mesoderm from the time of its formation during gastrulation and show that with the exception of the male perigonadal depot, visceral and subcutaneous adipocytes are derived from this tissue. Furthermore, we present evidence that APs of distinct ontogenies within the male perigonadal depot respond equivocally to a high fat diet (HFD) stimulus, despite clear positionally dependent responses along the anterior-posterior axis of the depot. Finally, we propose a unified model to describe adipocyte lineage relationships between and within depots and suggest that the depot-microenvironment, and not merely developmental history, is an important regulator of adipocyte lineage cell function.

Results

Tracing mesoderms of the whole somite, central dermomyotome and posterior lateral plate

Upon completion of gastrulation the mesodermal germ layer takes on a compartmentalized architecture with the somites and lateral plates comprising the bulk of the tissue. Somites are paired blocks of progenitor cells that form in parallel tracks along the anterior-posterior axis of the embryo and give rise predominately to vertebrae and muscle as well as a subset of dermis (Atit et al., 2006; Brent and Tabin, 2002; Buckingham et al., 2003). The central dermomyotome is contained within somitic mesoderm and is known to contribute to dermal and epaxial muscle lineages but not vertebral lineages (Atit et al., 2006; Lepper and Fan, 2010). Lateral plate mesoderm is physically unassociated with somites and forms as two bilaterally symmetric sac-like structures (Fig. 1a). These eventually generate, among other things, the serous membranes that line body cavities, the spleen and cardiovascular system (Brand, 2003; Thors and Drukker, 1997; Tribioli and Lufkin, 1999).

In order to distinguish the mesodermal subcompartments from which different adipose depots arise we first selected two Cre driver strains, Meox1-Cre and HoxB6-Cre, with mesodermal expression domains largely restricted to the somites (Jukkola et al., 2005) and lateral plates (Lowe et al., 2000), respectively. Moreover, it has been reported that interscapular brown adipocytes originate from $Pax7^{+}$ progenitors in the central dermomyotome (Lepper and Fan, 2010). However, this study utilized a cytoplasmic marker and did not trace BAT post-embryonically when adipocytes fill with lipid and become morphologically distinguishable from stromal cells. In contrast, we chose to perform lineage tracing experiments into adulthood with a Pax7-Cre knock-in that recapitulates the endogenous expression pattern of the Pax7 gene without disrupting Pax7 function (Keller et al., 2004). In all experiments we coupled the designated Cre recombinase with the mTmG reporter, which is highly effective in labeling adipocytes (Berry and Rodeheffer, 2013; Jeffery et al., 2014; Sanchez-Gurmaches and Guertin, 2014; Sanchez-Gurmaches et al., 2016). Briefly, the mTmG cassette tandemly encodes

membrane-localized tdTomato (mTomato) and membrane-localized GFP (mGFP) elements. In every cell where Cre recombinase is active the tdTomato element is excised thereby permitting expression of the GFP element; this indelibly switches the effected cell and its progeny from a red to a green fluorescent signature (Muzumdar et al., 2007).

To validate the reported mesodermal expression domains for these Cre lines we harvested several tissues known to be derived from either the somites or lateral plates from adult Meox1-Cre:mTmG (somite), Pax7-Cre:mTmG (central dermomyotome and myotome) and HoxB6-Cre:mTmG (lateral plate) animals. As expected, Meox1-Cre tracing strongly marked the somite-derived triceps and tibialis anterior muscles in mGFP but not the spleen or heart which arise from lateral plate mesoderm (Fig. 1b,c). The mesodermal expression domain for the Pax7 gene extends from central dermomyotome to the myotome in the embryo, ultimately being constrained to satellite cells in the adult (Relaix et al., 2005; Seale et al., 2000). As expected, Pax7-Cre tracing mirrors that of Meox1-Cre in these tissues (Fig. 1d,e). Thus, the Meox1-Cre:mTmG and Pax7-Cre:mTmG tracing systems label overlapping cell populations in the somites and derivatives thereof, but not lateral plate cells and their derivatives. HoxB6-Cre tracing did not appreciably label either skeletal muscles or the heart, but did strongly label the spleen in mGFP (Fig. 1f,g). The heart is derived from the anterior portion of the lateral plates (cardiac mesoderm) while the spleen is derived from the posterior portion (Brand, 2003; Onimaru et al., 2011; Roberts et al., 1994; Tribioli and Lufkin, 1999). Therefore, the HoxB6-Cre:mTmG system effectively labels posterior lateral plate mesoderm (PLPM) and its derivatives but not cardiac mesoderm or the somites and their derivatives.

Central dermomyotome contributes to a small subset of somite-derived adipocytes

After confirming that predicted adult tissues are labeled according to the reported mesodermal expression domains for Meox1-Cre, HoxB6-Cre and Pax7-Cre in our models, we applied these tools to better understand the developmental relationships among adipocyte lineages that populate major adipose depots. In all conditions whole adipose tissue was imaged by confocal microscopy and adipocytes designated as either mGFP$^+$ or mTomato$^+$ using ImageJ software (Schindelin et al., 2015; Schneider et al., 2012). In Meox1-Cre:mTmG animals major dorso-axial depots (i.e. retroperitoneal WAT, interscapular WAT and interscapular BAT) were labeled with mGFP, ranging from 85.9-96.2% of adipocytes depending on the depot (Fig. 2a,b,c). In contrast, virtually no adipocytes were traced in adipose depots positioned more peripherally and ventrally in the body (Fig. 2d,e,f,g). A striking exception, however, is the male perigonadal adipose depot in which 59.5% of adipocytes are mGFP$^+$. In females, only 4.2% of adipocytes display mGFP fluorescence, indicating the somites significantly contribute to the male but not female perigonadal adipocyte lineage. Interestingly, the Meox1-Cre tracing pattern of adipose tissue is very similar to the reported pattern for Pax3-Cre, from strong labeling of dorso-axial depots to the sexually dimorphic labeling of adipocytes in perigonadal fat (Sanchez-Gurmaches and Guertin, 2014). As Pax3 expression overlaps with Meox1 in the dermomyotome of somites (Relaix et al., 2005), these data suggest the mGFP$^+$ adipocytes in these tracing systems originate from progenitors in the dermomyotome.

Unlike Meox1 and Pax3, which are broadly expressed in the dermomyotome, Pax7 expression is restricted to progenitors in the central dermomyotome (Relaix et al., 2005). In the Pax7-Cre:mTmG tracing system less than 50% of adipocytes were labeled in interscapular white and brown depots (Fig. 3a,b) with no labeling in other depots examined (Fig. 3c,d,e,f,g). Since previous findings indicated that Pax7$^+$ progenitors contributed to all brown adipocytes present in late stage embryos (Lepper and Fan, 2010) it is possible that two distinct progenitor pools exist for brown adipocytes: one for establishing the

depot during organogenesis (Pax7^{+}) and one that infiltrates the depot and maintains the adipocyte lineage thereafter (Pax7^{-})(Jiang et al., 2014). If this were the case, we would predict a high percentage of brown adipocytes to be mGFP^{+} perinatally with a gradual decrease with age. To test this possibility, we compared the percentage of mGFP^{+} brown adipocytes in 1-2-day old pups with that observed in adults. We found no difference between these groups in adipocyte labeling or AP labeling, indicating Pax7^{+} embryonic progenitors contribute equally to the establishment and maintenance of the brown adipocyte population (Supp. Fig 1a,b). From these data, we also suggest that a minority of interscapular white and brown adipocytes arise from progenitors residing in the central dermomyotome with the rest being derived from a separate region of the dermomyotome.

Posterior lateral plate mesoderm (PLPM) contributes to subcutaneous and visceral adipocyte lineages

Since several adipose depots were untraced in the Meox1-Cre system we determined if adipocytes also arise from PLPM with the HoxB6-Cre:mTmG model. Indeed, we found remarkable complementarity in the tracing patterns for the Meox1-Cre:mTmG and HoxB6-Cre:mTmG systems with all depots being reciprocally labeled between them. HoxB6-Cre tracing showed virtually complete labeling of adipocytes in the inguinal subcutaneous depot as well as the mesenteric depot in both males and females (Fig. 4d,e,f) indicating that these visceral and subcutaneous WAT depots share a common developmental origin in the PLPM. The perigonadal depot again showed dramatic sexually dimorphic labeling with females having 99.8% mGFP^{+} adipocytes whereas males had a mere 5.3% (Fig 4g). This indicates the female perigonadal adipocyte lineage arises from PLPM, but that in males PLPM contributes only minimally to these cells. These data are consistent with previous findings showing that a substantial proportion of visceral adipocytes but not subcutaneous adipocytes, are derived from WT1^{+} progenitors between E14.5 and E16.5 (Chau et al., 2014). From these observations it was proposed that most visceral adipocytes arise from lateral plate mesoderm with a possible contribution from intermediate mesoderm (Chau et al., 2014). However, by E14.5 the lateral plate mesoderm and

intermediate mesoderm no longer exist (Diez-Roux et al., 2011) and their roles as tissues-of-origin can only be inferred. Furthermore, WT1-tracing was unable to inform an ontogeny for subcutaneous adipocytes and was performed exclusively in male mice, preventing the identification of sexual dimorphism among adipocyte lineages.

To test if adipocytes traced in the HoxB6-Cre:mTmG system arise from bona fide gastrulation-stage PLPM we utilized a tamoxifen-inducible tracing system (HoxB6-CreER^{T}:mTmG) to perform a pulse-chase experiment in which we transiently induced Cre activity at E8.5 when PLPM takes on its characteristic sac-like architecture (Lowe et al., 2000; Nguyen et al., 2009). At 4-6 weeks of age the adipose depots were harvested and analyzed for mGFP^{+}/mTomato^{+} adipocytes. We observed an overall reduction in mGFP^{+} cells in the inducible HoxB6-CreER^{T} system compared to the constitutive HoxB6-Cre system (Fig 4,5), which is likely due to the abbreviated window of Cre activity (~12 hrs) in the inducible system (Nakamura et al., 2006). Interestingly, the reduction in labeling was proportionally greater in the depot directly overlying the tricep (triWAT) relative to other depots (Fig 4d-g, 5d-g). This can be explained if triWAT (an internal though not visceral adipose depot) is mainly derived from the most antero-dorsal domain of PLPM, which appears not to have appreciable Cre activity in either tracing system at E8.5 (Lowe et al., 2000; Nguyen et al., 2009). Rather, triWAT labeling in the constitutive HoxB6-Cre system may be reflective of later Cre activity in the limb bud mesenchyme (Lowe et al., 2000). This would corroborate the pattern of tracing observed in the Prx1-Cre:mTmG model in which subcutaneous adipocytes closest to the forelimb display a greater proportion of Prx1 lineage tracing than those more dorsally positioned (Sanchez-Gurmaches et al., 2015). Taken as a whole, the tracing patterns for the constitutive and inducible HoxB6 systems largely mirror one another and support the notion that PLPM establishes adipocyte lineages that populate subcutaneous, internal and visceral adipose depots.

Anatomic distribution and developmental lineage-independent activity of adipocyte precursors (APs)

In conjunction with adipocyte tracing we quantified the percentage of mGFP$^+$/mTomato$^+$ APs residing in each depot via flow cytometry, according to their cell surface marker profile (CD45$^-$:CD31$^-$:CD29$^+$:CD34$^+$:Sca1$^+$:CD24$^{+/-}$)(Supp. Fig. 2a)(Berry and Rodeheffer, 2013; Rodeheffer et al., 2008). APs were designated mGFP$^+$ or mTomato$^+$ according to a stringent gating strategy (Supp. Fig. 2a) in which cells not meeting these criteria were designated unlabeled. Notably, double-positive (mGFP$^+$ and mTomato$^+$) APs were common in the inducible HoxB6-CreER^T:mTmG system which was likely because of mono-allelic recombination at the mTmG locus in homozygous animals. Thus, we included double-positive APs in the mGFP$^+$ count (Supp. Fig. 2b) as the presence of mGFP indicates Cre was active in an ancestor of those cells.

The depot-specific labeling patterns for APs in respective tracing systems mirrors patterns observed for adipocytes (Fig. 6), which indicates that embryonic progenitors from a given mesodermal subcompartment establish the AP and adipocyte populations in equal proportions for each adipose depot to which they contribute. To assess this relationship further we generated scatter plots in which mGFP$^+$ adipocytes and mGFP$^+$ APs from individual animals were plotted on the X and Y axes, respectively (Supp. Fig. 3). If the percentage of mGFP$^+$ adipocytes and APs are similar for a particular depot across different animals then data points will cluster together. If the percentage of mGFP$^+$ adipocytes and APs are similar in a single animal, but not across different animals, a linear relationship in data points for a given depot will be observed. Most depots follow one of these patterns in all tracing systems (Supp. Fig 3). However, the male perigonadal depot of the Meox1-Cre:mTmG system stands as a noteworthy exception. Here, mGFP$^+$ adipocyte populations range from 19.7% to 89% between animals whereas the mGFP$^+$ AP population is consistently around 50% in every animal analyzed (Supp. Fig 3a, orange). This observation can be explained if two conditions are met: (1) an unequal distribution of mGFP$^+$ (i.e.

somite-derived) adipocytes exists within the depot and (2) the quantification of somite-derived adipocytes was unintentionally skewed for each animal due to non-uniform sampling across the depot.

To test if somite-derived adipocytes and APs are differentially distributed in the male perigonadal depot we divided the depot into tip (anterior), middle, and base (posterior) and analyzed tracing for each region separately (Fig. 7a,b). Remarkably, we found a gradient of somite-derived adipocytes along the depot axis (Fig. 7c). In addition, APs follow the same pattern along the anterior-posterior axis of the depot with higher levels of somite-derived cells in the tip compared to the base (Fig. 7d). Adipocyte and AP tracing are concordant in each region of the depot (Fig. 7e). These data indicate that pooling APs from the whole depot, as in Figure 6, masked our ability to detect this aspect of patterning in the male perigonadal adipocyte lineage.

Given these observations we next aimed to gauge the relative contribution of ontogenetic and microenvironmental factors controlling the activity of APs that reside in a single depot yet are derived from different developmental lineages. We have previously shown that male perigonadal APs respond to HFD by proliferating and differentiating into adipocytes (Jeffery et al., 2015), but it is unclear if this response is biased to a particular AP lineage or region of the depot. We thus sought to identify if HFD-induced AP proliferation is influenced by the developmental origin or intra-depot location of APs by quantifying bromodeoxyuridine (BrdU) incorporation into these AP subpopulations upon HFD stimulus. Surprisingly, APs from the tip of the depot proliferate more in response to a HFD compared to those in the base (Fig. 7f). However, the APs from the somite-derived and non-somite-derived lineages proliferate at comparable rates throughout the depot (Fig. 7g), indicating that the regional response of APs to HFD within the male perigonadal depot is independent of developmental origin. Taken together, these data suggest that, under obesogenic conditions, the adipose tissue microenvironment overrides developmental origin effects on AP behavior in male perigonadal fat.

Discussion

Here we show adipocyte lineage tracing patterns for several Cre lines with well-defined mesodermal expression domains and leverage obesogenic AP proliferation to gauge functional differences between distinct AP lineages in the male perigonadal fat depot. We present evidence that indicates interscapular white and brown adipocyte lineages arise from somitic mesoderm, but only a minority of these cells arise from $Pax7^{+}$ progenitors in the central dermomyotome. Moreover, we demonstrate complementary labeling patterns in non-overlapping adipocyte lineages for the Meox1-Cre:mTmG and HoxB6-Cre:mTmG tracing systems. These data strongly suggest that both brown and white adipocytes of the dorso-axial adipocyte lineages, and a large proportion of the male perigonadal adipocyte lineage, arise from somitic mesoderm and therefore share a common progenitor pool with muscle. Whereas adipocyte lineages populating other major depots mainly originate from PLPM (Fig. 8a).

The finding that $Pax7^{+}$ progenitors of the central dermomyotome do not contribute to the majority of the interscapular brown adipocyte lineage is surprising given the intense staining of BAT observed by Lepper and Fan in late stage Pax7-$CreER^{T2}$:LacZ embryos (Lepper and Fan, 2010). A possible explanation for this discrepancy is the utilization of different reporters (LacZ vs mTmG), as noted previously. The use of different Cre strains could also contribute to this. Our group used a constitutive Pax7-Cre knock-in that does not disrupt endogenous Pax7 function (Keller et al., 2004), whereas the previous report used a knock-in strain that disrupts the Pax7 locus; animals were therefore heterozygous for a functional Pax7 gene in this tracing paradigm (Lepper and Fan, 2010), which could potentially alter lineage specification if gene dosage is affected (Buckingham and Relaix, 2007; Graf and Enver, 2009). Indeed, similar to our findings here, Atit and colleagues previously cited unpublished data suggesting not all BAT arises from progenitors of the central dermomyotome (Atit et al., 2006).

Meox1-Cre:mTmG lineage tracing in this study and the previously published adipocyte fate map for Pax3-Cre:mTmG (Sanchez-Gurmaches and Guertin, 2014) do, however, strongly suggest a dermomyotomal origin for cells of the interscapular adipocyte lineage (including those of the intrascapular WAT depot). In support of this notion, Myf5-Cre:mTmG tracing largely overlaps with Meox1-Cre and Pax3-Cre based paradigms, except there is no labeling of male perigonadal adipocytes in this system (Sanchez-Gurmaches and Guertin, 2014). It is known that Myf5 is expressed along a dorsoventral gradient in the dermomyotome with strongest expression in progenitors of the epaxial dermomyotome (Teboul et al., 2002). Indeed, Pax3 activity precedes and is required for Myf5 expression in the epaxial dermomyotome (Sato et al., 2010). Taking these observations together, we propose a fate map in which interscapular brown adipocytes predominately arise from a $Pax3^{+}/Myf5^{+}$-lineage originating in the epaxial dermomyotome, with a minor contribution from progenitors in the central dermomyotome that express Pax7, Pax3 and Myf5 as they proceed through development (Fig. 8b-d).

It follows that $Meox1^{Lin+}$ and $Pax3^{Lin+}$ adipocytes in the male perigonadal depot arise from hypaxial dermomyotome as neither Pax7 or Myf5 are appreciably expressed in this domain (Fig. 8a,b)(Lepper and Fan, 2010; Relaix et al., 2005; Sato et al., 2010; Teboul et al., 2002). Even so, the developmental origin for a significant proportion (35-40%) of male perigonadal adipocytes remains unclear. Since this depot is tightly associated with the epididymis, it is possible that these cells are derived from intermediate mesoderm, which is known to give rise to most organs of the urogenital tract (Davidson, 2009; Torres et al., 1995). However, precise lineage tracing tools that specifically mark intermediate mesoderm, and no other mesodermal subcompartments, will need to be developed in order to determine if this is the case. Moreover, inducible tracing from E8.5 with the HoxB6-$CreER^{T}$:mTmG system clearly demonstrates that several visceral adipocyte lineages share a common developmental origin in the PLPM with the inguinal subcutaneous adipocyte lineage. It is not until later

in fetal development, possibly during limb bud formation between E9.5 and E11.5 (Logan et al., 2002), when visceral ($WT1^{Lin+}$) and subcutaneous ($Prx1^{Lin+}$) adipocyte lineages diverge (Supp. Fig. 4)(Chau et al., 2014; Sanchez-Gurmaches et al., 2015).

Finally, the observation that HFD-induced AP proliferation in male perigonadal fat is positionally dependent, but not lineage-dependent, supports the notion that the depot microenvironment plays a significant role in AP behavior. Indeed, it has been shown that reciprocally transplanting APs between perigonadal and subcutaneous depots results in transplanted APs taking on the behavior of host-depot APs when challenged with HFD (Jeffery et al., 2016). This is particularly fascinating given that, in males, perigonadal and subcutaneous APs arise from distinct mesodermal progenitor pools. Despite these findings, it remains unknown what local signaling events are required to mediate the differential responses of APs to HFD within and between depots. Furthermore, whether the anterior-posterior gradient of somite-derived adipocyte lineage cells is functionally relevant in the adult or simply reflects developmental patterning is not clear.

Altogether, these data provide insight into the developmental ancestry of major adipose depots and show that AP behavior in the obesogenic conditions assessed here is reliant on microenvironmental factors not ontogeny. Further studies will be required to identify the mechanisms by which distinct adipocyte lineages are specified in the embryo and whether such lineage heterogeneity confers stable functional divergence among them. It will also be critical to account for crosstalk among adipocyte, hematopoietic and endothelial cell lineages between and within depots to further understand adipose tissue homeostasis and how it is deranged in diseases such as obesity and lipodystrophy.

Methods

Animals

Meox1-Cre mice(Jukkola et al., 2005) were a generous gift from Maria Barna, PhD at Stanford University. HoxB6-Cre (Lowe et al., 2000) and HoxB6-CreER^{T} mice (Nguyen et al., 2009) were generous gifts from Scott Weatherbee, PhD at Yale University. Pax7-Cre mice (Keller et al., 2004) (stock 010530) were acquired from Jackson Laboratory. Mice were 4-10 weeks of age unless otherwise noted. For AP proliferation assays, mice were treated with 0.8mg/ml BrdU (US Biological B2850) in drinking water for one week using lightproof bottles. Fresh BrdU water was administered every two days. For gestational tamoxifen treatment of HoxB6-CreER^{T}:mTmG mice, pregnant dams were intraperitoneally injected with 50mg/kg tamoxifen (Sigma T5648) and 25mg/kg progesterone (Sigma P3972) dissolved in vegetable oil at E8.5. Progesterone was co-administered with tamoxifen in order to offset tamoxifen's estrogenic activity in the uterus which can result in endometrial hyperplasia, late fetal abortion and dystocia (Nakamura et al., 2006; Shang and Brown, 2002). Standard chow diet was from Harlan Laboratories (2018S) and HFD from Research Diets (D12492). All experiments followed guidelines outlined by Yale University's Institutional Animal Care and Use Committee (IACUC).

Whole Mount and Confocal Imaging

Adipose depots were dissected and cut into ~1.5x1.5 cm chunks. These were immediately mounted onto microscope slides with Fluoromount-G (Southern Biotech 0100-01) and imaged on a Leica TCS SP5 confocal microscope. Images were taken with either 40x or 20x objectives and cropped to scale accordingly. Brightness and contrast were adjusted for select images to improve the visibility of cell membranes and mGFP^{+}/mTomato^{+} adipocytes were quantified using the multi-point tool in ImageJ software (Schindelin et al., 2015; Schneider et al., 2012).

Flow Cytometry

Adipose tissue digestion and isolation of stromal vascular cells was performed as described previously (Berry and Rodeheffer, 2013; Church et al., 2014; Jeffery et al., 2015). These cells were then stained with the following antibodies on ice in the dark for 30-60 minutes in 1X Hank's Buffered Salt Solution (HBSS)(Gibco 14185-052) + 3% bovine serum albumin (BSA)(AmericanBio 9048-46-8): CD29 Alexa Fluor 700 (BioLegend, 102218, clone HMβ1-1 used at 1:400), CD31 PE-Cy7 (eBioscience, 25-0311-82, clone 390, used at 1:1000), Sca-1 V450 (BD Biosciences, 560653, clone D7, used at 1:500), CD45 APC-eFluor 780 (eBioscience, 47-0451-80, clone 30-F11, used at 1:2000), CD24 PerCP-Cyanine 5.5 (eBioscience, 45-0242-82, clone M1/69, used at 1:400), CD34 Alexa Fluor 647 (BioLegend, 119314, clone MEC14.7, used at 1:400). Following antibody staining, the cells were washed with HBSS + 3% BSA and analyzed on a BD LSRII flow cytometer. For BrdU analysis, the same tissue digestion procedure was carried out as noted above. Cells were then stained with the following antibodies for 30 minutes on ice in the dark: CD29 Alexa Fluor 700 (BioLegend, 102218, clone HMβ1-1 used at 1:400), CD31 PE-Cy7 (eBioscience, 25-0311-82, clone 390, used at 1:500), Sca-1 V500 (BD Biosciences, 561229, clone D7, used at 1:250), CD45 APC-eFluor 780 (eBioscience, 47-0451-80, clone 30-F11, used at 1:500). Following this, cells were washed in HBSS + 3% BSA, then fixed and permeabilized with Phosflow Lyse/Fix (BD Biosciences 558049) and Perm Buffer III (BD Biosciences 558050) according to the manufacturer's instructions. Cells were then treated with DNase (Deoxyribonuclease I, Worthington, ~500 units/ml) in dPBS with calcium and magnesium (Sigma D8662) for 90 minutes in a 37°C water bath. Cells were washed in HBSS + 3% BSA and stained overnight in the dark at 4°C with anti-BrdU antibody (Alexa Fluor 647, Phoenix Flow Systems, AX647, clone 3D4, used at 1:30). The next day, cells were washed with HBSS + 3% BSA and stained with the following antibodies for 60 minutes at room temperature in the dark: CD24 PerCP-Cyanine 5.5 (eBioscience, 45-0242-82, clone M1/69, used at 1:200), CD34 Brilliant Violet 421 (BioLegend, 119321, clone MEC14.7, used at 1:400), CD29 Alexa Fluor 700 (BioLegend, 102218, clone HMβ1-1 used at 1:400),

CD31 PE-Cy7 (eBioscience, 25-0311-82, clone 390, used at 1:500), Sca-1 V500 (BD Biosciences, 561229, clone D7, used at 1:250), CD45 APC-eFluor 780 (eBioscience, 47-0451-80, clone 30-F11, used at 1:500).

Statistical Analysis

Statistical analyses are denoted in each figure legend. All tests were performed using GraphPad Prism version 7.0. Data are presented as mean ± SEM and $P < 0.05$ was considered statistically significant. A minimum number of 3 biological replicates (i.e. 3 mice) were used for each experiment. Experiments were not blinded as genotypes of mice were known prior to analysis. Samples were excluded if mice displayed fight wounds, appeared otherwise unhealthy or if technical error occurred during an experimental procedure.

Acknowledgments

This work was supported by a National Science Foundation Graduate Research Fellowship DGE1122492 to Z.L.S., and NIDDK grants DK090489 and DK110147 to M.S.R. We also thank Zuzana Tobiasova of the Yale Stem Cell Center FACS Core and Thomas Ardito of the Yale Stem Cell Center Confocal Microscope Core for technical assistance and advice in flow cytometry and confocal microscopy, respectively.

References

Atit, R., Sgaier, S. K., Mohamed, O. A., Taketo, M. M., Dufort, D., Joyner, A. L., Niswander, L. and Conlon, R. A. (2006). β-catenin activation is necessary and sufficient to specify the dorsal dermal fate in the mouse. *Developmental biology* **296**, 164-176.

Berry, R. and Rodeheffer, M. S. (2013). Characterization of the adipocyte cellular lineage in vivo. *Nature cell biology* **15**, 302.

Brand, T. (2003). Heart development: molecular insights into cardiac specification and early morphogenesis. *Developmental biology* **258**, 1-19.

Brent, A. E. and Tabin, C. J. (2002). Developmental regulation of somite derivatives: muscle, cartilage and tendon. *Current opinion in genetics & development* **12**, 548-557.

Buckingham, M., Bajard, L., Chang, T., Daubas, P., Hadchouel, J., Meilhac, S., Montarras, D., Rocancourt, D. and Relaix, F. (2003). The formation of skeletal muscle: from somite to limb. *Journal of anatomy* **202**, 59-68.

Buckingham, M. and Relaix, F. (2007). The role of Pax genes in the development of tissues and organs: Pax3 and Pax7 regulate muscle progenitor cell functions. *Annu. Rev. Cell Dev. Biol.* **23**, 645-673.

Cannon, B. and Nedergaard, J. (2004). Brown adipose tissue: function and physiological significance. *Physiological reviews* **84**, 277-359.

Chau, Y.-Y., Bandiera, R., Serrels, A., Martínez-Estrada, O. M., Qing, W., Lee, M., Slight, J., Thornburn, A., Berry, R. and McHaffie, S. (2014). Visceral and subcutaneous fat have different origins and evidence supports a mesothelial source. *Nature cell biology* **16**, 367-375.

Church, C. D., Berry, R. and Rodeheffer, M. S. (2014). Isolation and study of adipocyte precursors. In *Methods in enzymology*, pp. 31-46: Elsevier.

Cypess, A. M., Lehman, S., Williams, G., Tal, I., Rodman, D., Goldfine, A. B., Kuo, F. C., Palmer, E. L., Tseng, Y.-H. and Doria, A. (2009). Identification and importance of brown adipose tissue in adult humans. *New England Journal of Medicine* **360**, 1509-1517.

Davidson, A. J. (2009). Mouse kidney development.

de Jong, J. M., Larsson, O., Cannon, B. and Nedergaard, J. (2015). A stringent validation of mouse adipose tissue identity markers. *American Journal of Physiology-Endocrinology and Metabolism* **308**, E1085-E1105.

Diez-Roux, G., Banfi, S., Sultan, M., Geffers, L., Anand, S., Rozado, D., Magen, A., Canidio, E., Pagani, M. and Peluso, I. (2011). A high-resolution anatomical atlas of the transcriptome in the mouse embryo. *PLoS biology* **9**, e1000582.

Graf, T. and Enver, T. (2009). Forcing cells to change lineages. *Nature* **462**, 587.

Jeffery, E., Berry, R., Church, C. D., Yu, S., Shook, B. A., Horsley, V., Rosen, E. D. and Rodeheffer, M. S. (2014). Characterization of Cre recombinase models for the study of adipose tissue. *Adipocyte* **3**, 206-211.

Jeffery, E., Church, C. D., Holtrup, B., Colman, L. and Rodeheffer, M. S. (2015). Rapid depot-specific activation of adipocyte precursor cells at the onset of obesity. *Nature cell biology* **17**, 376.

Jeffery, E., Wing, A., Holtrup, B., Sebo, Z., Kaplan, J. L., Saavedra-Peña, R., Church, C. D., Colman, L., Berry, R. and Rodeheffer, M. S. (2016). The adipose tissue microenvironment regulates depot-specific adipogenesis in obesity. *Cell metabolism* **24**, 142-150.

Jiang, Y., Berry, D. C., Tang, W. and Graff, J. M. (2014). Independent stem cell lineages regulate adipose organogenesis and adipose homeostasis. *Cell reports* **9**, 1007-1022.

Jukkola, T., Trokovic, R., Maj, P., Lamberg, A., Mankoo, B., Pachnis, V., Savilahti, H. and Partanen, J. (2005). Meox1Cre: a mouse line expressing Cre recombinase in somitic mesoderm. *Genesis* **43**, 148-153.

Keller, C., Hansen, M. S., Coffin, C. M. and Capecchi, M. R. (2004). Pax3: Fkhr interferes with embryonic Pax3 and Pax7 function: implications for alveolar rhabdomyosarcoma cell of origin. *Genes & development* **18**, 2608-2613.

Khan, T., Muise, E. S., Iyengar, P., Wang, Z. V., Chandalia, M., Abate, N., Zhang, B. B., Bonaldo, P., Chua, S. and Scherer, P. E. (2009). Metabolic dysregulation and adipose tissue fibrosis: role of collagen VI. *Molecular and cellular biology* **29**, 1575-1591.

Lang, D., Lu, M. M., Huang, L., Engleka, K. A., Zhang, M., Chu, E. Y., Lipner, S., Skoultchi, A., Millar, S. E. and Epstein, J. A. (2005). Pax3 functions at a nodal point in melanocyte stem cell differentiation. *Nature* **433**, 884.

Lee, M.-J., Wu, Y. and Fried, S. K. (2013). Adipose tissue heterogeneity: implication of depot differences in adipose tissue for obesity complications. *Molecular aspects of medicine* **34**, 1-11.

Lepper, C. and Fan, C. M. (2010). Inducible lineage tracing of Pax7-descendant cells reveals embryonic origin of adult satellite cells. *Genesis* **48**, 424-436.

Logan, M., Martin, J. F., Nagy, A., Lobe, C., Olson, E. N. and Tabin, C. J. (2002). Expression of Cre Recombinase in the developing mouse limb bud driven by a Prxl enhancer. *genesis* **33**, 77-80.

Lowe, L. A., Yamada, S. and Kuehn, M. R. (2000). HoxB6-Cre transgenic mice express Cre recombinase in extra-embryonic mesoderm, in lateral plate and limb mesoderm and at the midbrain/hindbrain junction. *Genesis* **26**, 118-120.

Marcelin, G., Ferreira, A., Liu, Y., Atlan, M., Aron-Wisnewsky, J., Pelloux, V., Botbol, Y., Ambrosini, M., Fradet, M. and Rouault, C. (2017). A PDGFRα-Mediated Switch toward CD9 high Adipocyte Progenitors Controls Obesity-Induced Adipose Tissue Fibrosis. *Cell metabolism* **25**, 673-685.

Muzumdar, M. D., Tasic, B., Miyamichi, K., Li, L. and Luo, L. (2007). A global double-fluorescent Cre reporter mouse. *genesis* **45**, 593-605.

Nakamura, E., Nguyen, M. T. and Mackem, S. (2006). Kinetics of tamoxifen-regulated Cre activity in mice using a cartilage-specific CreERT to assay temporal activity windows along the proximodistal limb skeleton. *Developmental dynamics* **235**, 2603-2612.

Nedergaard, J., Bengtsson, T. and Cannon, B. (2007). Unexpected evidence for active brown adipose tissue in adult humans. *American Journal of Physiology-Endocrinology and Metabolism* **293**, E444-E452.

Nguyen, M. T., Zhu, J., Nakamura, E., Bao, X. and Mackem, S. (2009). Tamoxifen-dependent, inducible Hoxb6CreERT recombinase function in lateral plate and limb mesoderm, CNS isthmic organizer, posterior trunk neural crest, hindgut, and tailbud. *Developmental Dynamics* **238**, 467-474.

Onimaru, K., Shoguchi, E., Kuratani, S. and Tanaka, M. (2011). Development and evolution of the lateral plate mesoderm: comparative analysis of amphioxus and lamprey with implications for the acquisition of paired fins. *Developmental biology* **359**, 124-136.

Relaix, F., Rocancourt, D., Mansouri, A. and Buckingham, M. (2005). A Pax3/Pax7-dependent population of skeletal muscle progenitor cells. *Nature* **435**, 948.

Roberts, C. W., Shutter, J. R. and Korsmeyer, S. J. (1994). Hox11 controls the genesis of the spleen. *Nature* **368**, 747.

Rodeheffer, M. S., Birsoy, K. and Friedman, J. M. (2008). Identification of white adipocyte progenitor cells in vivo. *Cell* **135**, 240-249.

Rosen, E. D. and Spiegelman, B. M. (2014). What we talk about when we talk about fat. *Cell* **156**, 20-44.

Rupnick, M. A., Panigrahy, D., Zhang, C.-Y., Dallabrida, S. M., Lowell, B. B., Langer, R. and Folkman, M. J. (2002). Adipose tissue mass can be regulated through the vasculature. *Proceedings of the National Academy of Sciences* **99**, 10730-10735.

Sanchez-Gurmaches, J. and Guertin, D. A. (2014). Adipocytes arise from multiple lineages that are heterogeneously and dynamically distributed. *Nature communications* **5**, 4099.

Sanchez-Gurmaches, J., Hsiao, W.-Y. and Guertin, D. A. (2015). Highly selective in vivo labeling of subcutaneous white adipocyte precursors with Prx1-Cre. *Stem cell reports* **4**, 541-550.

Sanchez-Gurmaches, J., Hung, C.-M. and Guertin, D. A. (2016). Emerging complexities in adipocyte origins and identity. *Trends in cell biology* **26**, 313-326.

Sato, T., Rocancourt, D., Marques, L., Thorsteinsdóttir, S. and Buckingham, M. (2010). A Pax3/Dmrt2/Myf5 regulatory cascade functions at the onset of myogenesis. *PLoS genetics* **6**, e1000897.

Schindelin, J., Rueden, C. T., Hiner, M. C. and Eliceiri, K. W. (2015). The ImageJ ecosystem: An open platform for biomedical image analysis. *Molecular reproduction and development* **82**, 518-529.

Schneider, C. A., Rasband, W. S. and Eliceiri, K. W. (2012). NIH Image to ImageJ: 25 years of image analysis. *Nature methods* **9**, 671.

Seale, P., Bjork, B., Yang, W., Kajimura, S., Chin, S., Kuang, S., Scime, A., Devarakonda, S., Conroe, H. M. and Erdjument-Bromage, H. (2008). PRDM16 controls a brown fat/skeletal muscle switch. *Nature* **454**, 961-967.

Seale, P., Sabourin, L. A., Girgis-Gabardo, A., Mansouri, A., Gruss, P. and Rudnicki, M. A. (2000). Pax7 is required for the specification of myogenic satellite cells. *Cell* **102**, 777-786.

Shang, Y. and Brown, M. (2002). Molecular determinants for the tissue specificity of SERMs. *Science* **295**, 2465-2468.

Shen, W., Wang, Z., Punyanita, M., Lei, J., Sinav, A., Kral, J. G., Imielinska, C., Ross, R. and Heymsfield, S. B. (2003). Adipose tissue quantification by imaging methods: a proposed classification. *Obesity* **11**, 5-16.

Tallquist, M. D., Weismann, K. E., Hellstrom, M. and Soriano, P. (2000). Early myotome specification regulates PDGFA expression and axial skeleton development. *Development* **127**, 5059-5070.

Teboul, L., Hadchouel, J., Daubas, P., Summerbell, D., Buckingham, M. and Rigby, P. W. (2002). The early epaxial enhancer is essential for the initial expression of the skeletal muscle determination gene Myf5 but not for subsequent, multiple phases of somitic myogenesis. *Development* **129**, 4571-4580.

Thors, F. and Drukker, J. (1997). Serous membranes and their development, structure, and topography. In *Peritoneal adhesions*, pp. 3-13: Springer.

Torres, M., Gómez-Pardo, E., Dressler, G. R. and Gruss, P. (1995). Pax-2 controls multiple steps of urogenital development. *Development* **121**, 4057-4065.

Tribioli, C. and Lufkin, T. (1999). The murine Bapx1 homeobox gene plays a critical role in embryonic development of the axial skeleton and spleen. *Development* **126**, 5699-5711.

Xu, H., Barnes, G. T., Yang, Q., Tan, G., Yang, D., Chou, C. J., Sole, J., Nichols, A., Ross, J. S. and Tartaglia, L. A. (2003). Chronic inflammation in fat plays a crucial role in the development of obesity-related insulin resistance. *The Journal of clinical investigation* **112**, 1821-1830.

Zhou, B., Ma, Q., Rajagopal, S., Wu, S. M., Domian, I., Rivera-Feliciano, J., Jiang, D., von Gise, A., Ikeda, S. and Chien, K. R. (2008). Epicardial progenitors contribute to the cardiomyocyte lineage in the developing heart. *Nature* **454**, 109.

Figures

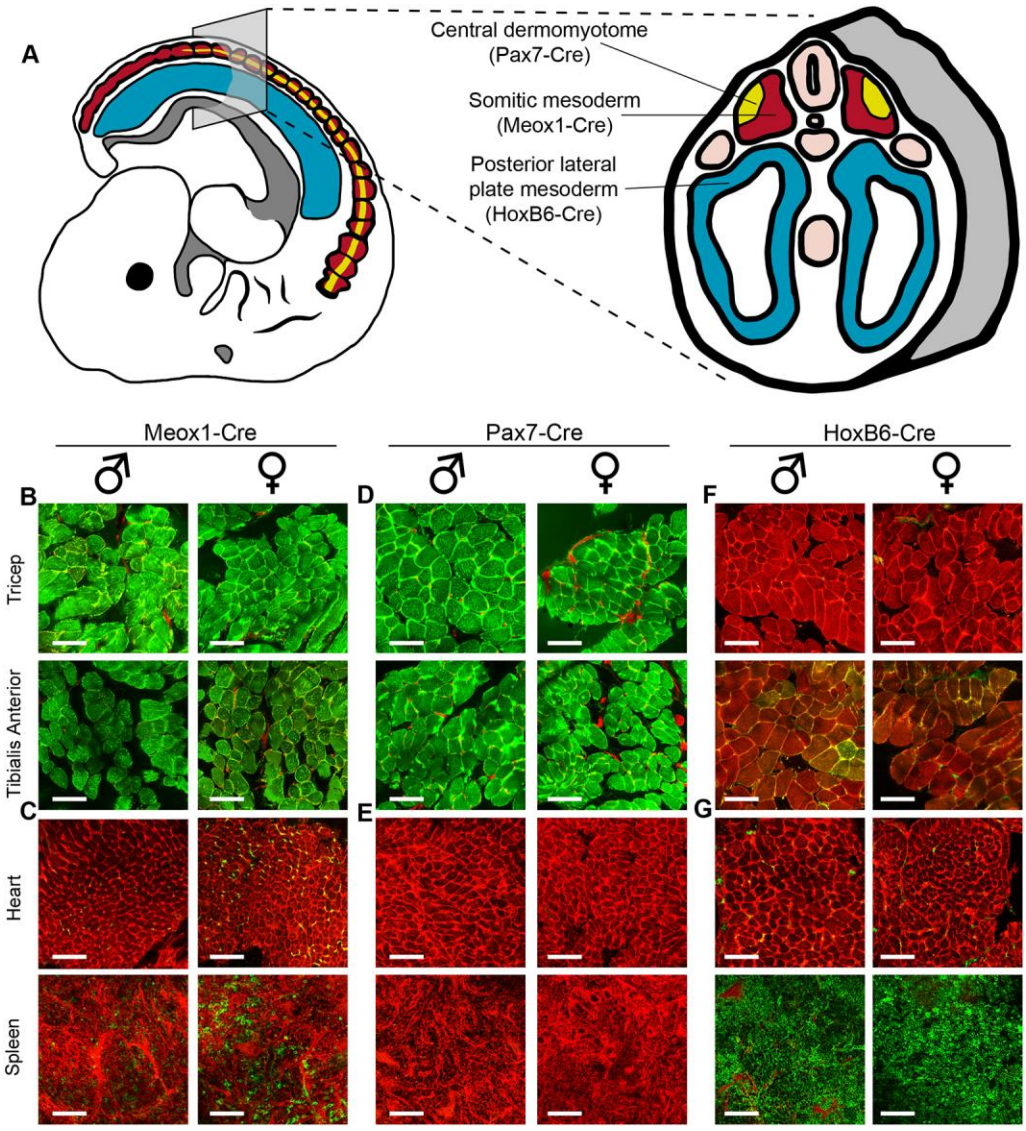

Figure 1. Fate-mapping mesodermal subcompartments using the Cre/Lox system. (A) Cre drivers used in this study and the unique mesodermal subcompartments in which they are active. (B) tracing of somite-derived tissues (triceps and tibialis anterior) in the Meox1-Cre:mTmG system. (C) tracing of anterior lateral plate (heart) and posterior lateral plate (spleen) derived tissue in the Meox1-Cre:mTmG system. (D) Same as B except in the Pax7-Cre:mTmG system. (E) Same as C except in the Pax7-Cre:mTmG

system. (F) Same as B and D except using the HoxB6-Cre:mTmG system. (G) Same as C and C except using the HoxB6-Cre:mTmG system. Data are from males and females 4-10 weeks of age. Scale bar is 100 um.

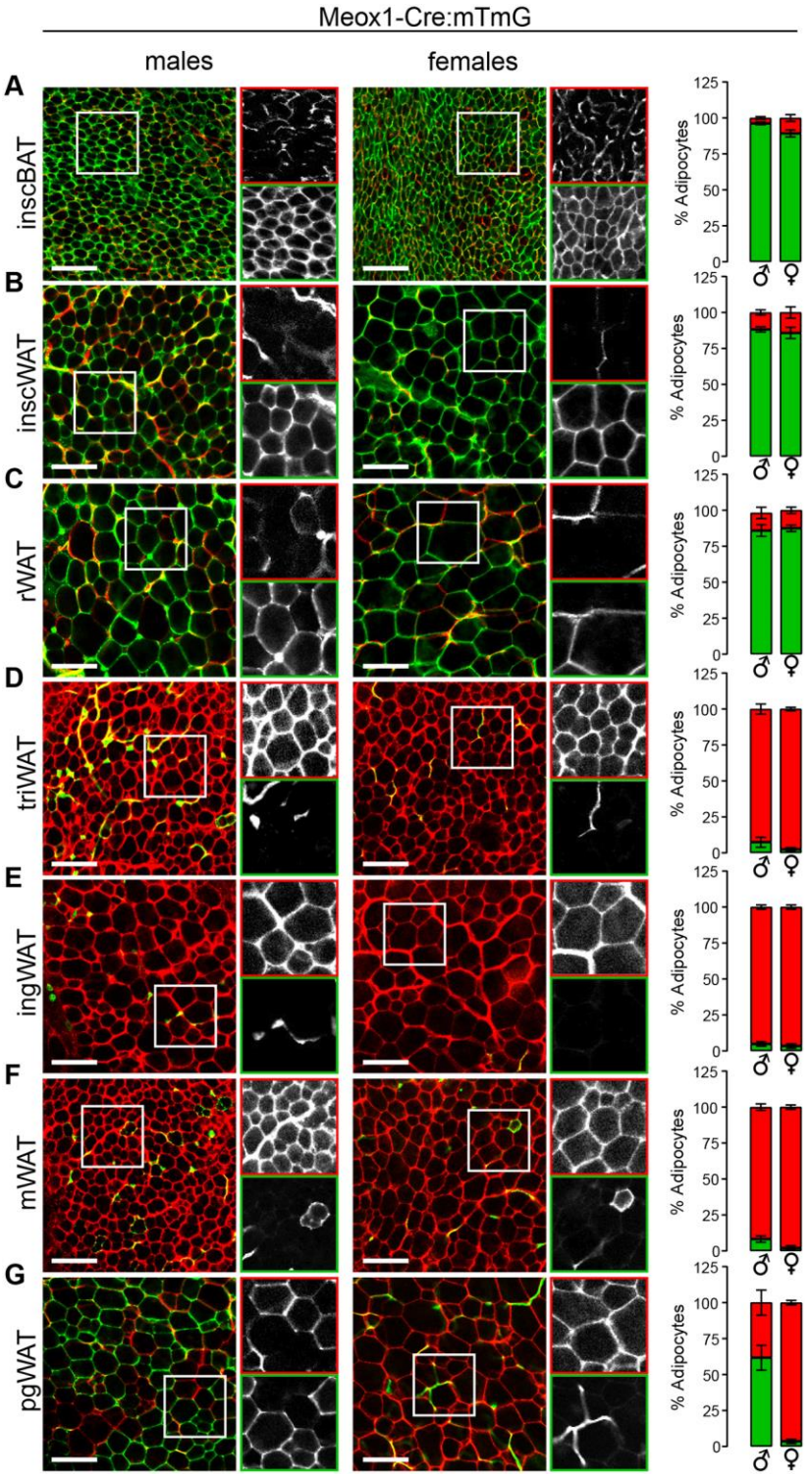

Figure 2. Meox1-CremTmG tracing: dorso-axial adipocytes and male perigonadal adipocytes predominately arise from somitic mesoderm. (A) Interscapular brown adipose tissue (inscBAT). (B) Interscapular white adipose tissue (inscWAT). (C) retroperitoneal white adipose tissue (rWAT). (D) triceps white adipose tissue (triWAT). (E) inguinal white adipose tissue (ingWAT). (F) mesenteric white adipose tissue (mWAT). (G) perigonadal white adipose tissue (pgWAT). n=6-8 depending on the depot. Data are from males 4-6 weeks of age and females 5-6 weeks of age. For each image, the black and white subsets indicate red (top) or green (bottom) channels. Error bars represent mean ± SEM. Scale bar is 100 um.

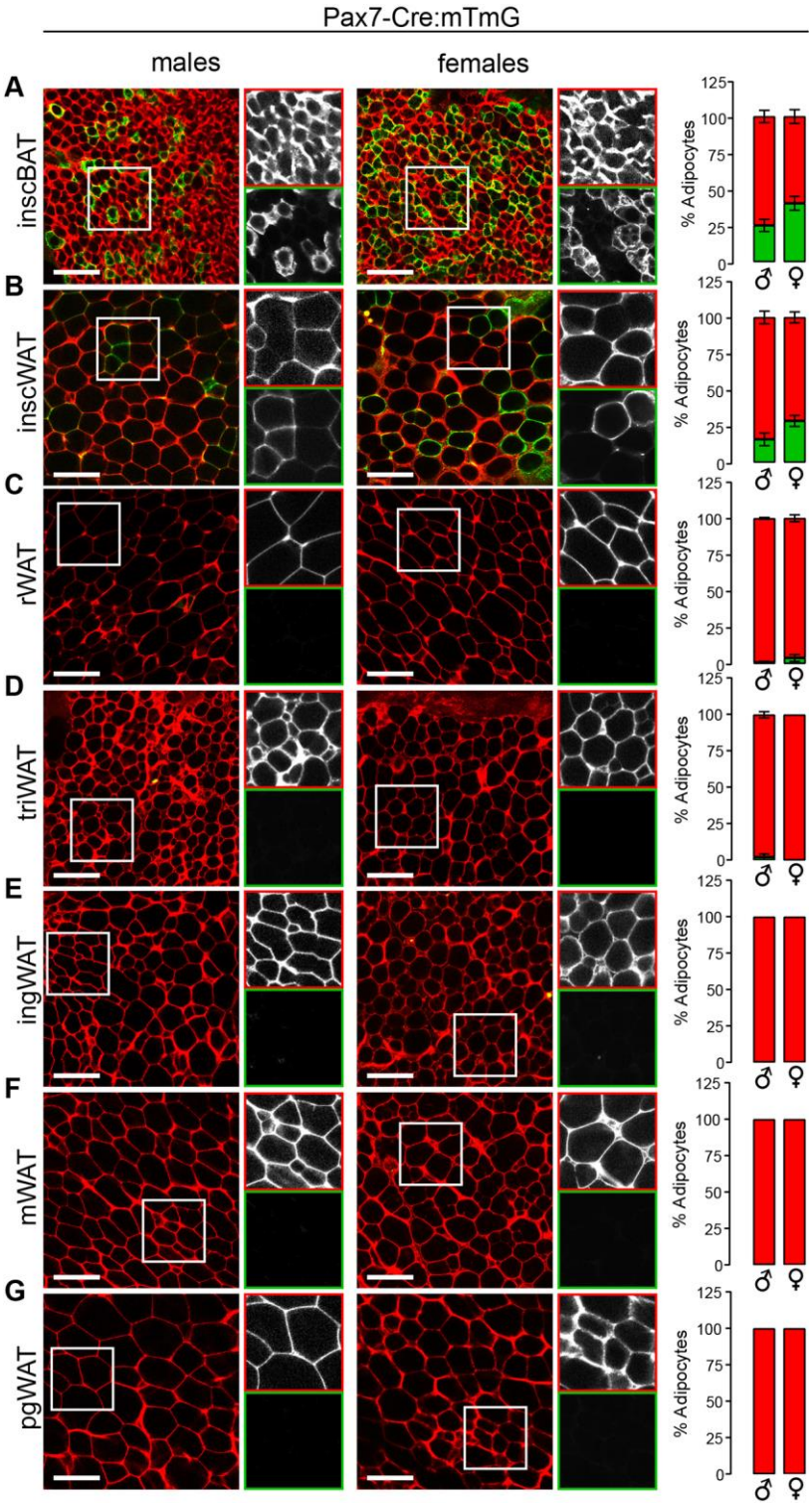

Figure 3. Pax7-Cre:mTmG tracing: a minority of interscapular white and brown adipocytes originate in the central dermomyotome. (A) Interscapular brown adipose tissue (inscBAT). (B) Interscapular white adipose tissue (inscWAT). (C) retroperitoneal white adipose tissue (rWAT). (D) triceps white adipose tissue (triWAT). (E) inguinal white adipose tissue (ingWAT). (F) mesenteric white adipose tissue (mWAT). (G) perigonadal white adipose tissue (pgWAT). n=3-7 depending on the depot. Data are from males 4-10 weeks of age and females 4-9 weeks of age. For each image, the black and white subsets indicate red (top) or green (bottom) channels. Error bars represent mean ± SEM. Scale bar is 100 um.

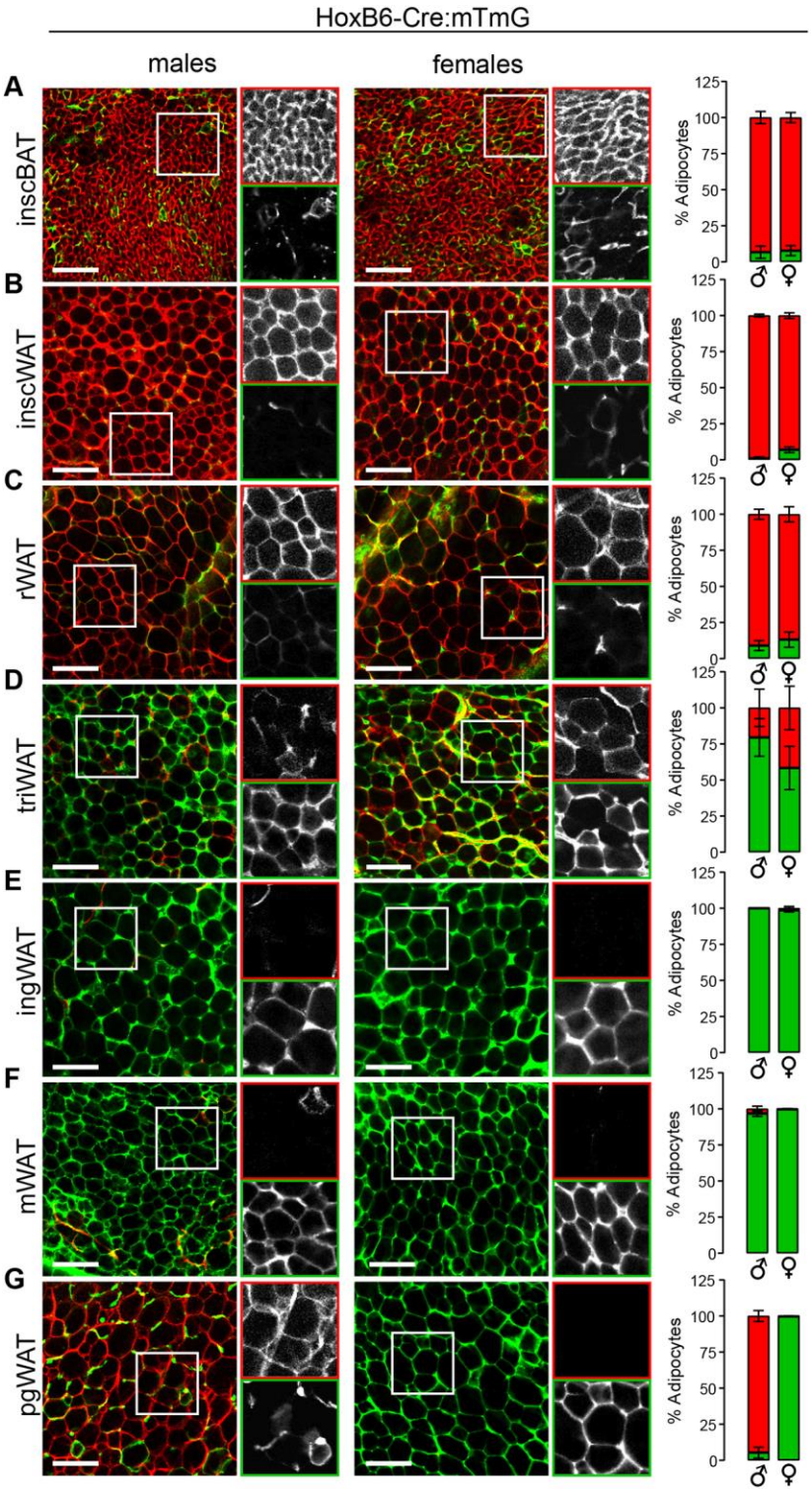

Figure 4. HoxB6-Cre:mTmG tracing: adipocytes populating major ventro-lateral adipose depots share a common lineage. (A) Interscapular brown adipose tissue (inscBAT). (B) Interscapular white adipose tissue (inscWAT). (C) retroperitoneal white adipose tissue (rWAT). (D) triceps white adipose tissue (triWAT). (E) inguinal white adipose tissue (ingWAT). (F) mesenteric white adipose tissue (mWAT). (G) perigonadal white adipose tissue (pgWAT). n=4-6 depending on the depot. Data are from males 5 weeks ± 3 days of age and females 5-7 weeks of age. For each image, the black and white subsets indicate red (top) or green (bottom) channels. Error bars represent mean ± SEM. Scale bar is 100 um.

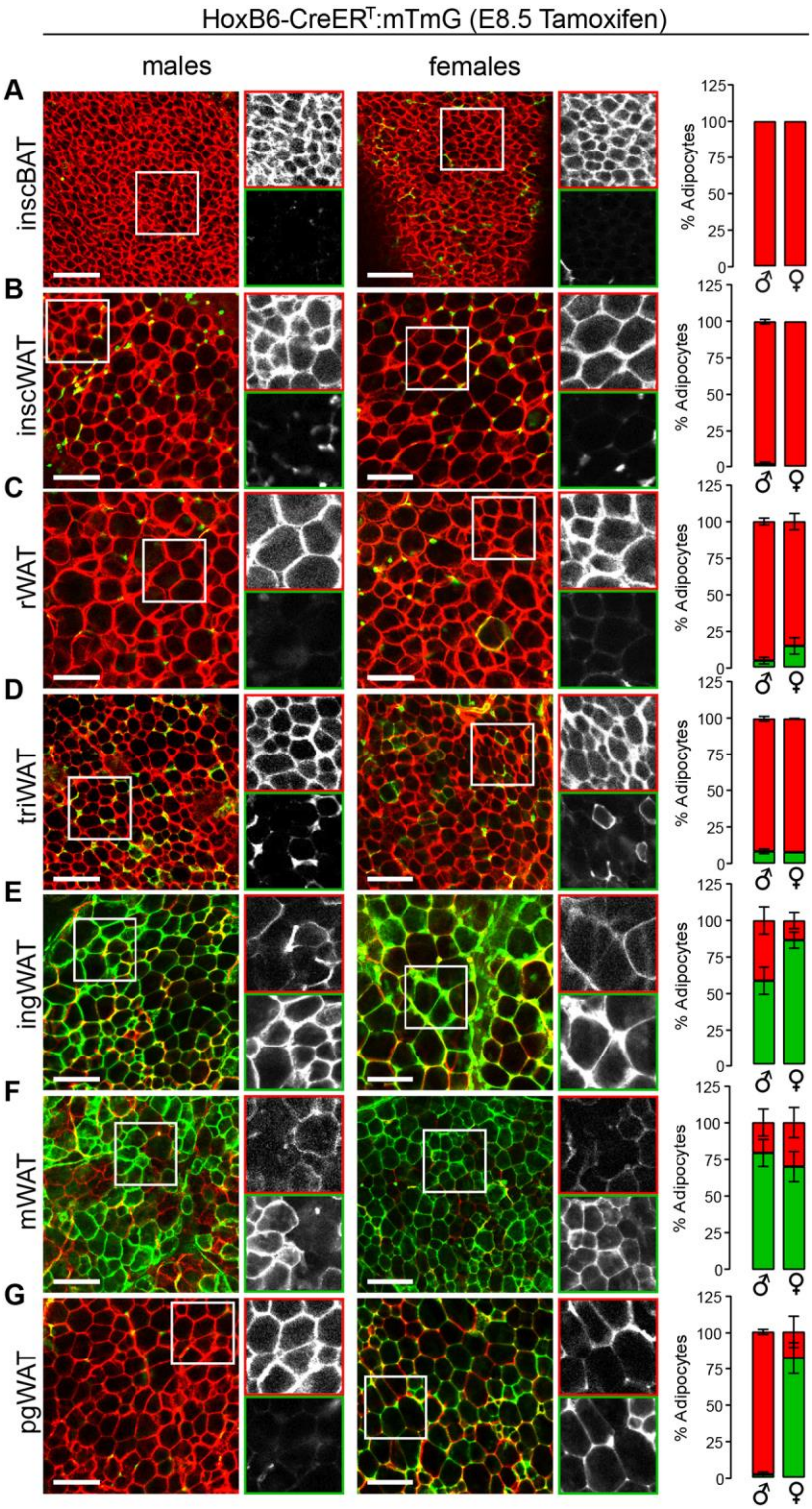

Figure 5. HoxB6-CreER^{T}:mTmG tracing: posterior lateral plate mesoderm establishes ventro-lateral adipocytes. (A) Interscapular brown adipose tissue (inscBAT). (B) Interscapular white adipose tissue (inscWAT). (C) retroperitoneal white adipose tissue (rWAT). (D) triceps white adipose tissue (triWAT). (E) inguinal white adipose tissue (ingWAT). (F) mesenteric white adipose tissue (mWAT). (G) perigonadal white adipose tissue (pgWAT). n=3-5 depending on the depot. Data are from males 5 weeks ± 2 days of age and females 4-5 weeks of age. For each image, the black and white subsets indicate red (top) or green (bottom) channels. Error bars represent mean ± SEM. Scale bar is 100 um.

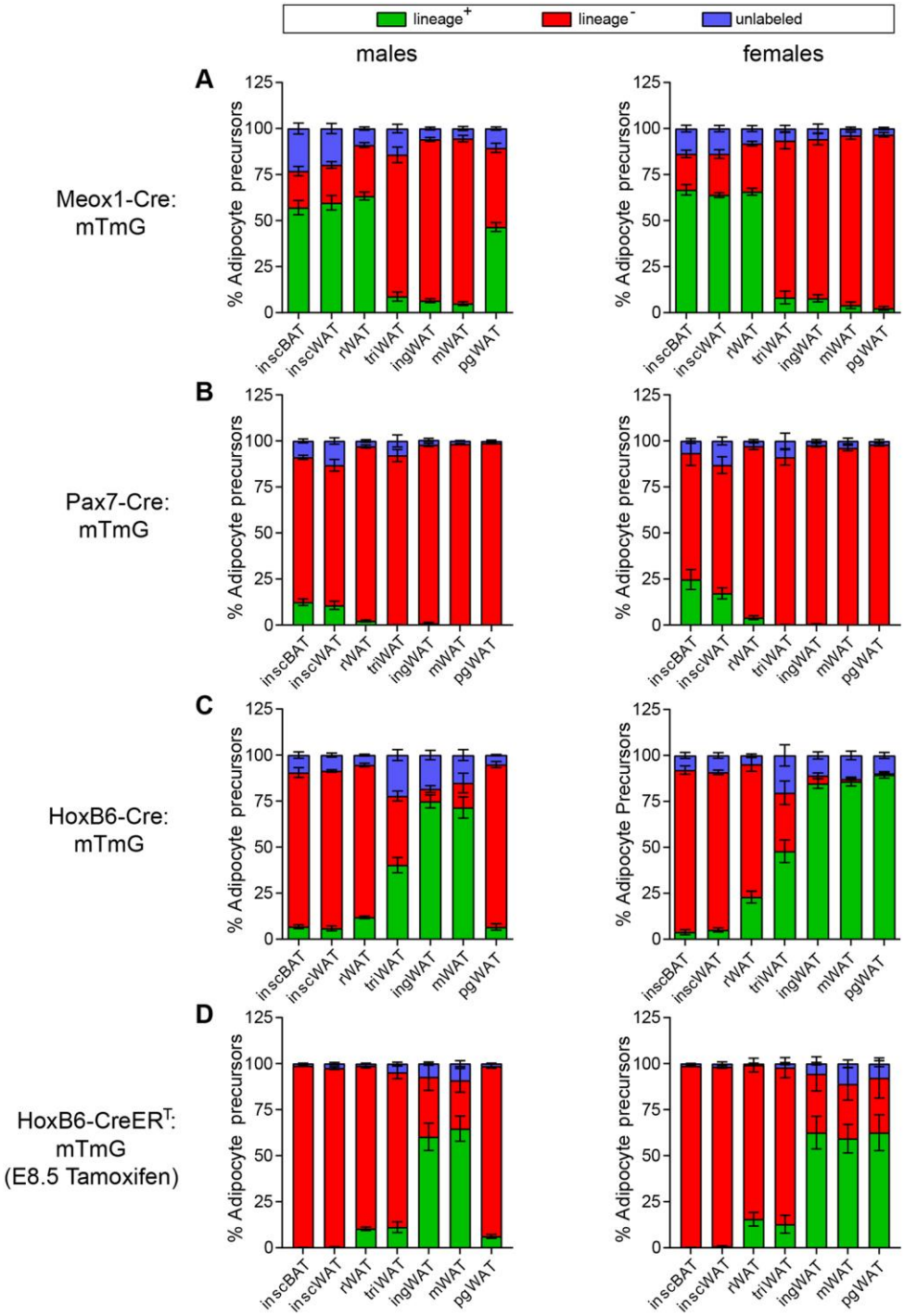

Figure 6. Lineage tracing patterns for depot-resident adipocyte precursors (APs). (A) Meox1-Cre:mTmG AP tracing in males (n=7-8) and females (n=6-7) for seven major adipose depots. (B) Pax7-Cre:mTmG AP tracing in males (n=5-7) and females (n=3-5) for seven major adipose depots. (C) HoxB6-Cre:mTmG AP tracing in males (n=4) and females (n=5-6) for seven major adipose depots. (D) HoxB6-CreERT:mTmG AP tracing in males (n=4) and females (n=3-5) for seven major adipose depots. Green denotes mGFP+ APs, red denotes mTomato+ APs and blue denotes unlabeled APs according to the gating strategy shown in Supplemental Figure 2A, B.

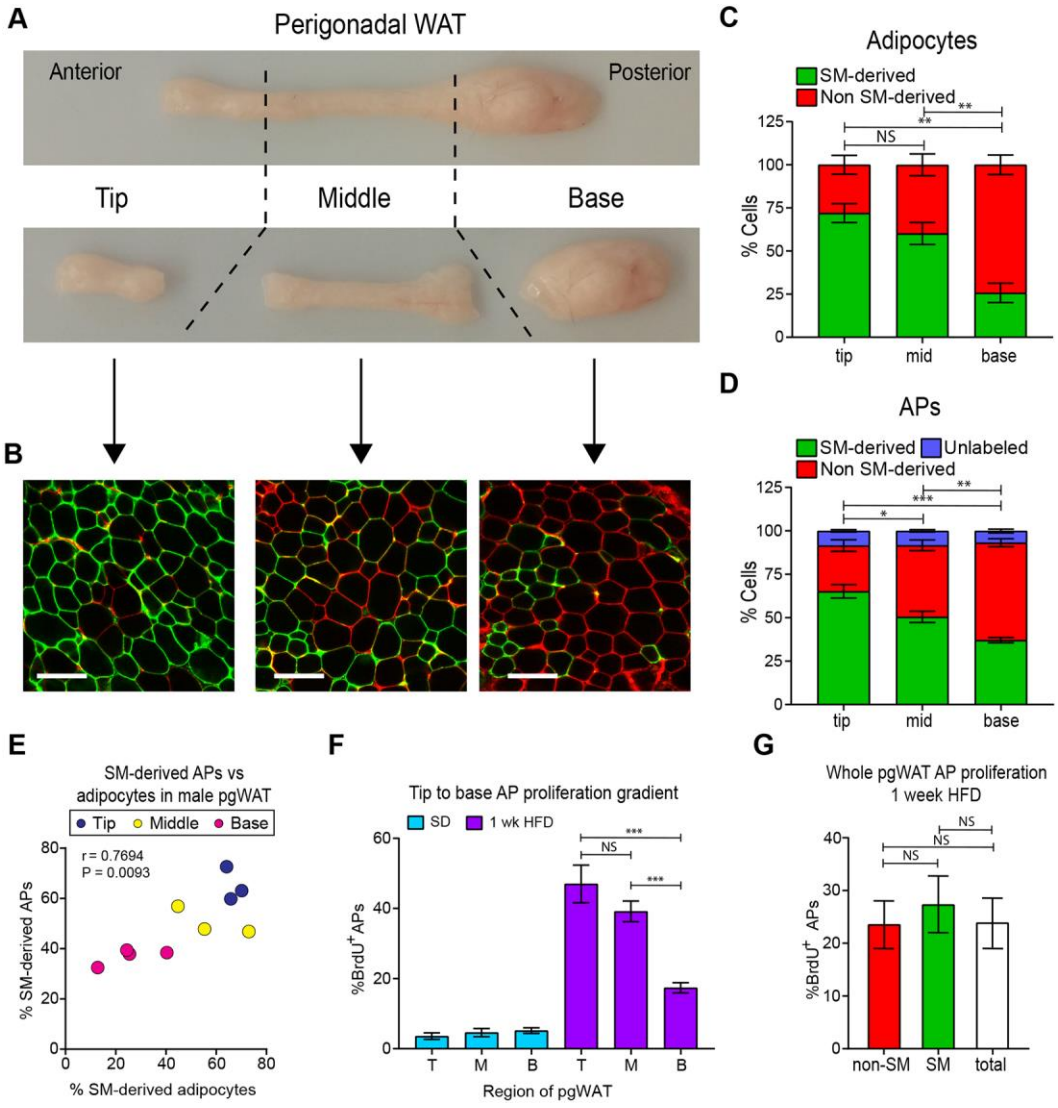

Figure 7. The tissue microenvironment, not developmental lineage, controls obesogenic AP proliferation in male perigonadal fat. (A) Anatomy of male perigonadal white adipose tissue (pgWAT) with tip, middle and base indicated. (B) Representative confocal images of tip, middle and base of pgWAT from male Meox1-Cre:mTmG animals. (C) Quantification of $mGFP^+$/$mTomato^+$ adipocytes in noted regions of male Meox1-Cre:mTmG pgWAT (n=4). (D) Quantification of $mGFP^+$/$mTomato^+$ APs in noted regions of male Meox1-Cre:mTmG pgWAT (n=3-4). (E) Scatterplot indicating concordant tracing of adipocytes and APs in each region of male Meox1-Cre:mTmG pgWAT. Each dot represents the percent of APs and adipocytes that are $mGFP^+$ for the indicated region of the depot in one animal (n=3-4). Since the pgWAT depot exists in a pair, one depot was used for quantifying adipocyte labeling and the other for AP labeling. Adipocyte labeling alone is shown in Figure 7C and AP labeling alone is shown in Figure 7D. (F) BrdU incorporation into APs of tip, middle and base of male pgWAT after 1 week of high fat diet (n=5). (G) BrdU incorporation into somite derived ($mGFP^+$) and non-somite derived ($mTomato^+$) APs of male Meox1-Cre:mTmG pgWAT (n=6). Significance in C, D, F and G was determined by comparing the indicated groups using an unpaired two-tailed Student's t test. SM = somitic mesoderm. Significance in E was determined using Pearson's two-tailed correlation analysis. In C and D $mGFP^+$ cells were used to calculate significance. Error bars represent mean ± SEM. *($P<0.05$), **($P<0.01$), ***($P<0.001$). NS = not significant. Scale bar is 100 um.

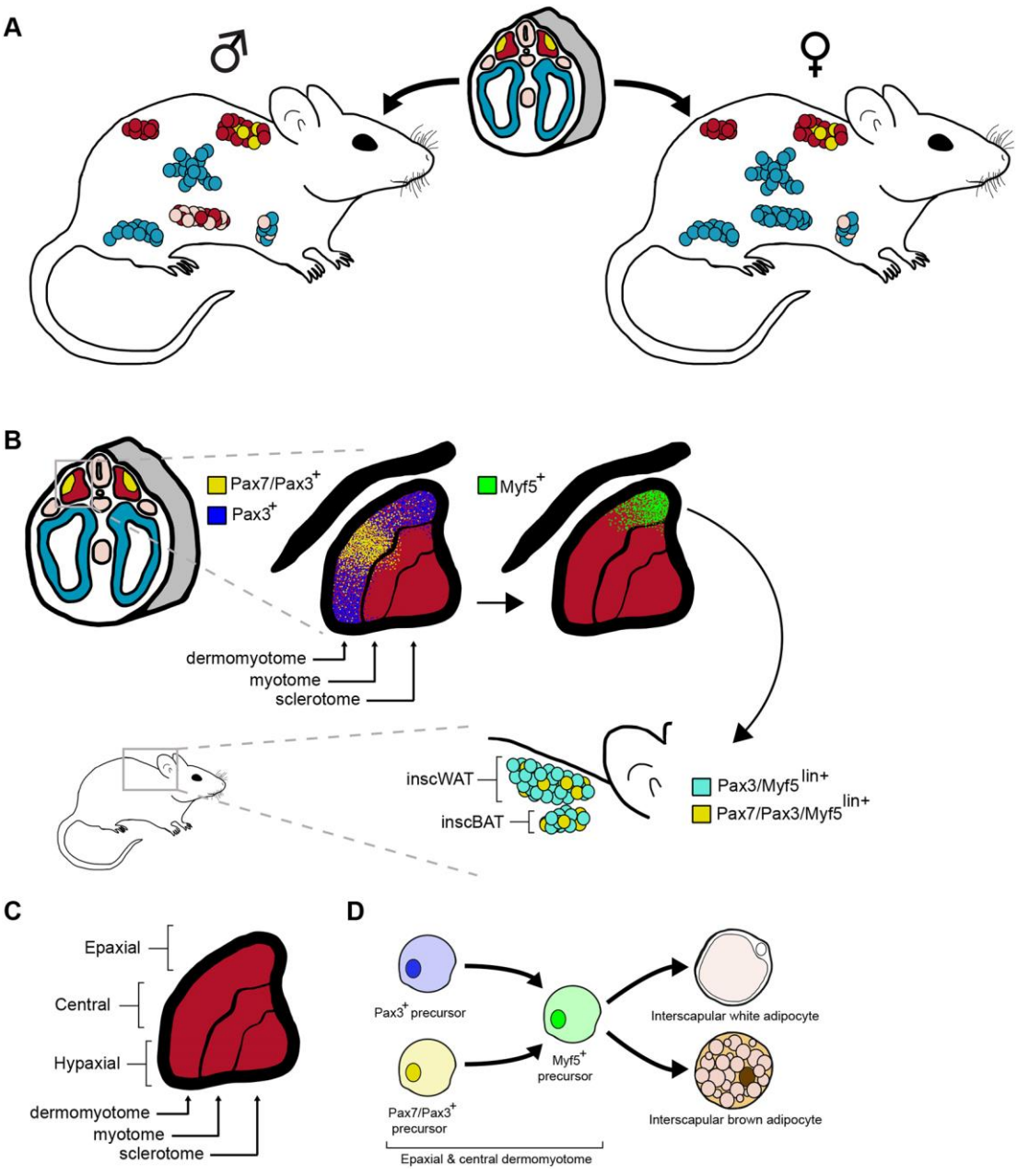

Figure 8. A mesodermal fate map for adipose tissue. (A) Schematic showing the mesodermal fate map for adipose tissue based on tracing with Meox1-Cre:mTmG, Pax7-Cre:mTmG and HoxB6-Cre:mTmG systems. Somitic mesoderm and derivative adipocyte lineages are in crimson; central dermomyotome and derivative adipocyte lineages are in yellow; posterior lateral plate mesoderm and derivative adipocyte lineages are in teal. (B) Schematic showing a model fate map for interscapular adipocyte

lineages based on Pax7-Cre:mTmG tracing in this study and Pax3/Myf5-Cre:mTmG tracing by Sanchez-Gurmaches et al. (Sanchez-Gurmaches and Guertin, 2014) (C) Schematic of somite subcompartments. (D) Model lineage hierarchy for interscapular adipocytes based on Pax7-Cre:mTmG tracing in this study and Pax3/Myf5-Cre:mTmG tracing by Sanchez-Gurmaches et al. (Sanchez-Gurmaches and Guertin, 2014).

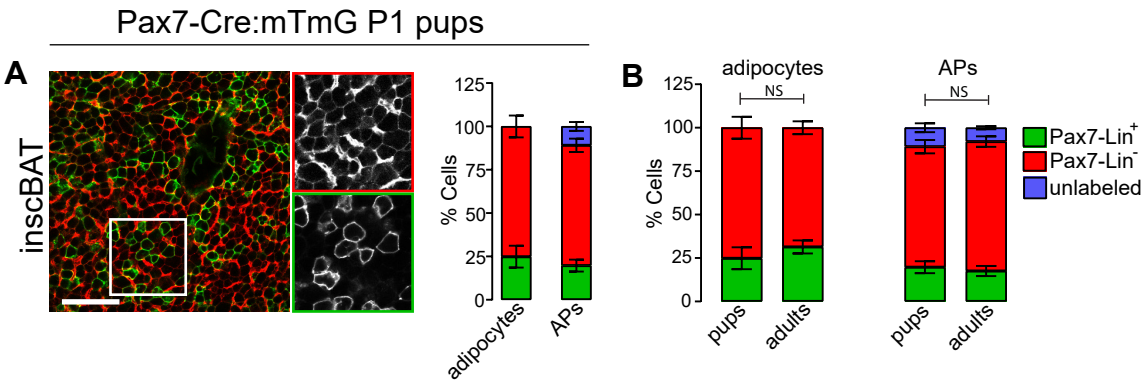

Supplementary Figure 1. Pax7^{Lin+} cells contribute equally to neonatal and adult brown adipocyte lineages. (A) Representative confocal image of brown fat from a 1 day old Pax7-Cre:mTmG pup with quantification of adipocyte and AP labeling. (B) Comparison of adipocyte and AP labeling between 1 day old pup adult Pax7-Cre:mTmG animals from Figure 3. Data from males and females was pooled for pups and adults. The black and white subset images indicate red (top) or green (bottom) channels. n=4 pups, n=12 adults. Error bars indicate mean ± SEM. NS = not significant. Scale bar is 100 um.

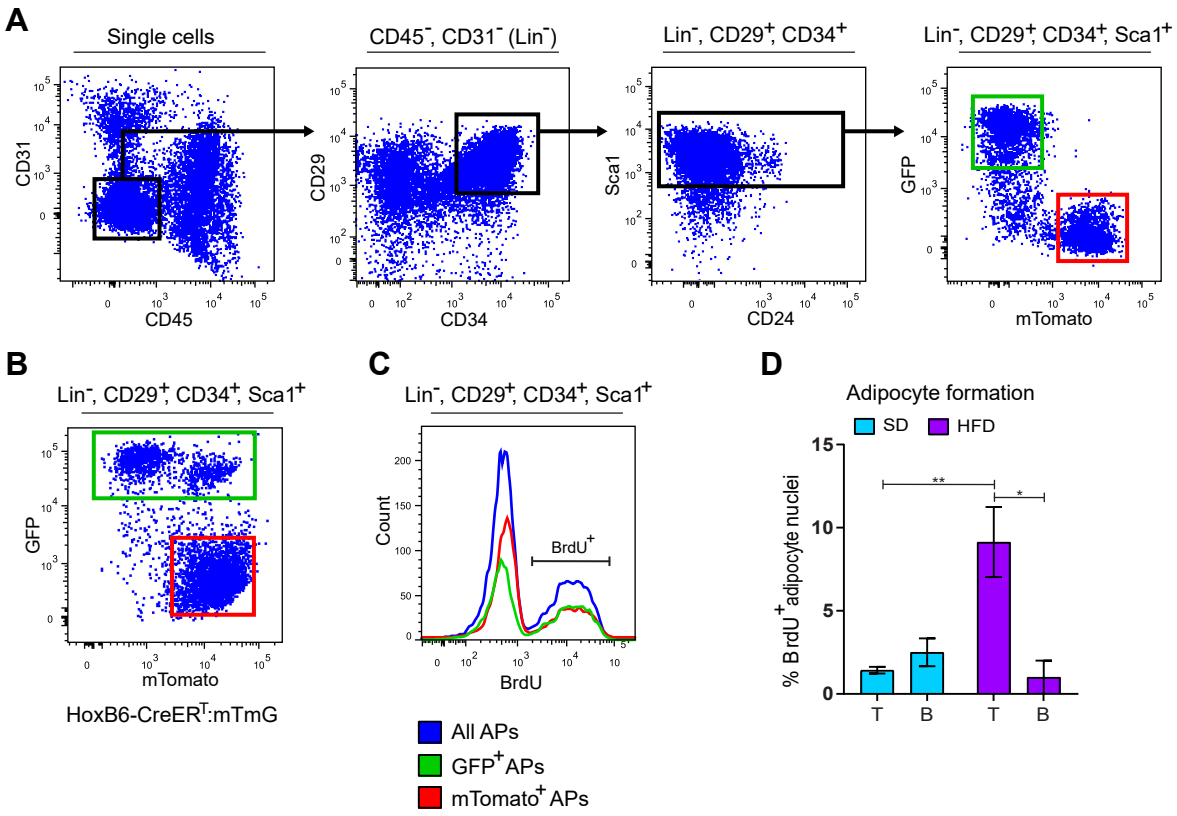

Supplementary Figure 2. Representative flow cytometry analysis of APs and adipogenesis in male perigonadal fat. (A) Representative flow plot for the identification of mGFP+ and mTomato+ APs in constitutive Cre strains. (B) Representative flow plot of mGFP+, mTomato+ and mGFP/mTomato double-positive APs in the inducible HoxB6-CreERT:mTmG strain. (C) Method for quantifying BrdU incorporation into APs of distinct lineages. (D) Percent adipocytes arising from proliferative APs in the tip and base of male perigonadal fat (n = 4-5). Adipose tissue was imbedded in paraffin, sectioned and immunostained for BrdU following 1 week of BrdU treatment (pulse) and seven additional weeks of the indicated diet (chase). Sections were imaged via a Leica TCS SP5 confocal microscope and BrdU+ adipocyte nuclei were manually quantified in each condition. SD = standard diet, HFD = high fat diet. *(P<0.05), **(P<0.01). Statistical significance was determined using an unpaired Student's t test for indicated groups.

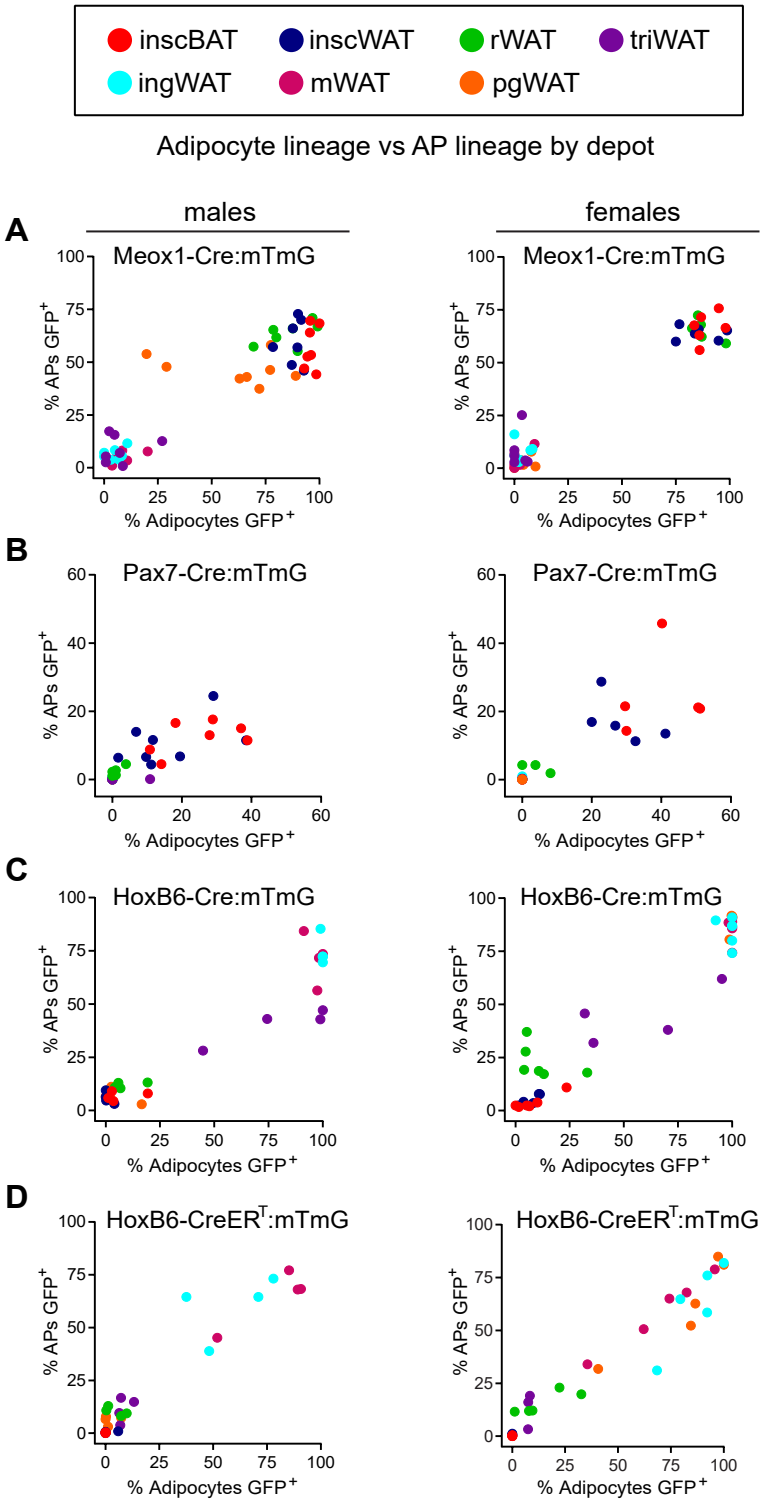

Supplementary Figure 3. Depot-specific adipocyte and AP labeling are largely concordant across tracing paradigms. Each scatter plot shows percent mGFP+ adipocytes on the x-axis and percent mGFP+ APs on the y-axis. Each adipose depot is denoted by a single color (red = inscBAT, blue = inscWAT, green = rWAT, purple = triWAT, teal = ingWAT, magenta = mWAT, orange = pgWAT). Each dot represents a single biological replicate (i.e. one animal). Given that each adipose depot exists in a pair, one depot was used for quantifying adipocyte labeling and the other was used to quantify AP tracing per animal. Adipocyte tracing is presented alone in figures 2 through 5. AP tracing is presented alone in figure 6. Data from males and females are shown for each tracing paradigm. (A) Meox1-Cre:mTmG. (B) Pax7-Cre:mTmG. (C) HoxB6-Cre:mTmG. (D) HoxB6-CreERT:mTmG. inscBAT = interscapular brown adipose tissue, inscWAT = interscapular white adipose tissue, rWAT = retroperitoneal white adipose tissue, triWAT = triceps white adipose tissue, ingWAT = inguinal white adipose tissue, mWAT = mesenteric white adipose tissue, pgWAT = perigonadal white adipose tissue.

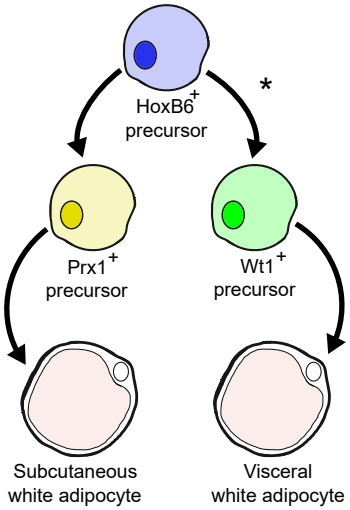

Supplementary Figure 4. Model cell lineage hierarchy for subcutaneous and visceral adipocytes. Based on HoxB6-Cre:mTmG and HoxB6-CreERT:mTmG tracing in this study as well as Prx1-Cre:mTmG and WT1-Cre:mTmG tracing from Sanchez-Gurmaches et al. (Sanchez-Gurmaches et al., 2015) and Chau et al. (Chau et al., 2014), respectively. The asterisk denotes the exception of male perigonadal adipocytes which predominately arise from Pax3 $^{Lin+}$/Meox1 $^{Lin+}$ progenitors in the somites.

References

Chau, Y.-Y., Bandiera, R., Serrels, A., Martínez-Estrada, O. M., Qing, W., Lee, M., Slight, J., Thornburn, A., Berry, R. and McHaffie, S. (2014). Visceral and subcutaneous fat have different origins and evidence supports a mesothelial source. Nature cell biology 16, 367.

Sanchez-Gurmaches, J., Hsiao, W.-Y. and Guertin, D. A. (2015). Highly selective in vivo labeling of subcutaneous white adipocyte precursors with Prx1-Cre. Stem cell reports 4, 541-550.

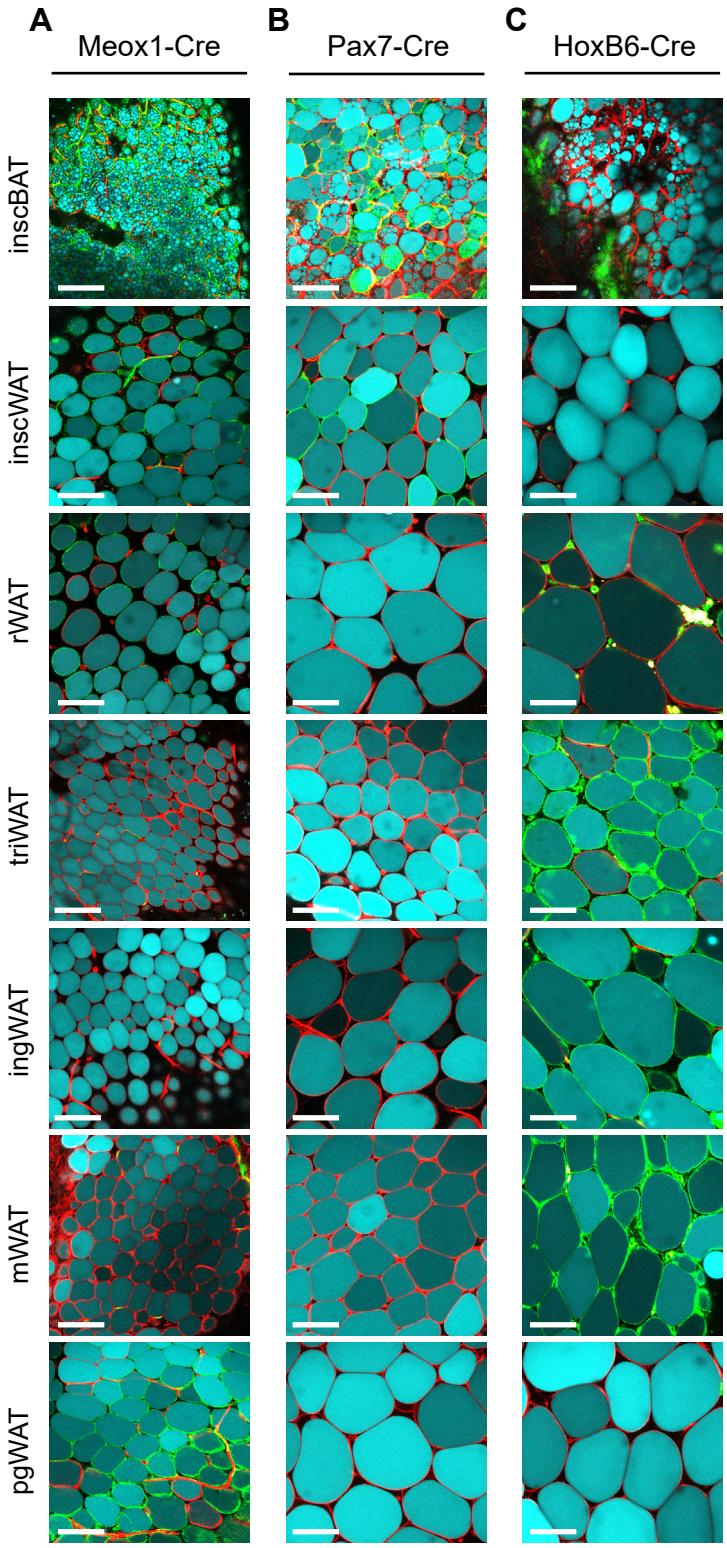

Supplementary Figure 5. Lipid staining of adipocytes in lineage tracing systems. Approximately 1.5x1.5 cm chunks of each adipose depot were dissected and stained with LipidTOX Deep Red (Invitrogen H34477) in PBS for 1 hr at room temperature. Following this incubation, tissue was washed once in PBS and mounted for confocal imaging as described in the "Whole Mount and Confocal Imaging" section. (A) Meox1-Cre:mTmG adipose tissue from an ~7 month old male. (B) ~10 month old Pax7-Cre:mTmG male. (C) ~10 month old HoxB6-Cre:mTmG male. Scale bar = 100 um.

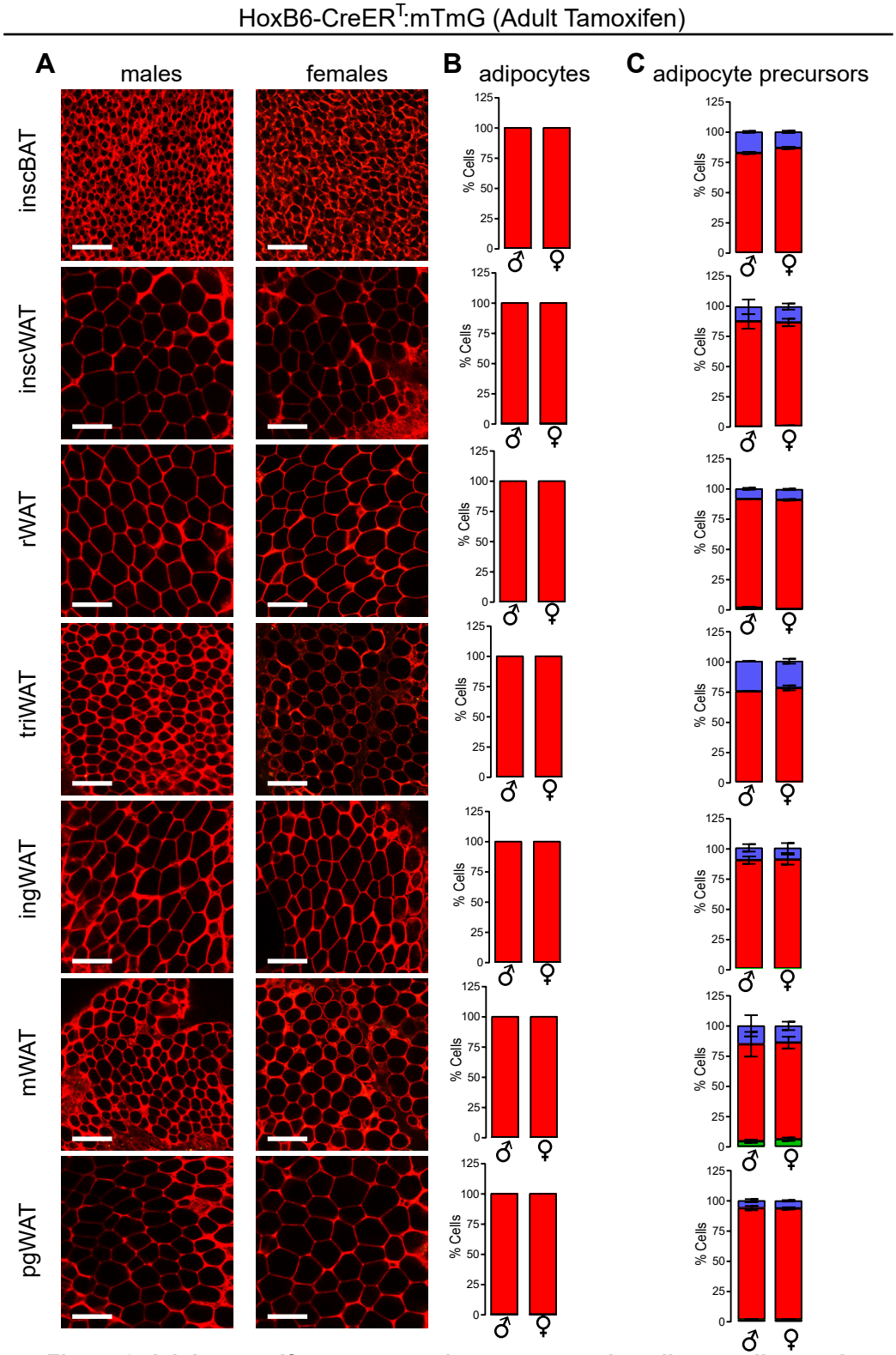

Supplementary Figure 6. Adult tamoxifen treatment does not trace the adipocyte lineage in HoxB6-CreER^{T}:mTmG animals. Mice were intraperitoneally injected with 50mg/kg tamoxifen in vegetable oil once a day for five days; 72 hours later, animals were sacrificed and adipose tissue harvested. (A) representative images of indicated adipose depots. (B) quantification of mGFP+ and mTomato+ adipocytes. (C) quantification of mGFP+ and mTomato+ adipocyte precursors. Data are from males (n = 2) and females (n = 2) of ~7.5 months of age. Adipocyte tracing was analyzed by confocal microscopy and adipocyte precursor tracing was analyzed by flow cytometry. Error bars represent mean ± SEM. Scale bar = 100 um.